

The effect of lattice strain on catalytic activity

E.E. Westsson¹, S.J. Picken¹, G.J.M. Koper¹

¹Technical University of Delft, The Netherlands

Supporting Information

1. Introduction In current commercial Proton Exchange Membrane (PEM) fuel cells Platinum is used as a catalyst speeding up the oxygen reduction reaction (ORR) taking place on the cathode. Fuel cells are generally considered to be a promising environmentally friendly energy conversion technology, since electricity can be generated by combining hydrogen and oxygen electrochemically releasing only water as exhaust product. Despite a number of degradation issues ¹, Platinum has long been considered the best oxygen reduction catalyst amongst the pure metals, commonly demonstrated by Volcano-type plots ² semi-logarithmically displaying catalytic activity versus intermediate binding affinity. It is worth noting that the oxygen reduction is a multiple step reaction with specific binding energies between the substrate and oxygen reduction intermediates for every step throughout the 4-electron reduction, for which the exact reaction path is still being discussed ^{2, 3}. Pt(111) comes close to an “optimal” binding energy for one of the proposed intermediates, namely Pt-O, but could nevertheless not be entitled the ideal catalyst simply because the other binding energies are less optimal.

Fitting a thin layer of Platinum onto another metal is bound to have consequences for the electronic properties of the Pt shell, both geometrically through lattice mismatch and electronically through shifting of the d-band and, as a consequence, the binding energies for e.g. the oxygen reduction intermediates ⁴⁻⁶. Similarly, hydrogen adsorption and desorption on Platinum is expected to be influenced by the distorted lattice. Because of this, the common way of calculating the electrochemically active surface area (ECSA) is likely to be little representative. This is because ECSA is estimated using the method, described in e.g. ^{7, 8}, based on the charge associated with adsorption and desorption of hydrogen on a bulk Platinum surface, the Platinum loading on the electrode and an estimated Coulombic charge required to desorb hydrogen from Platinum.

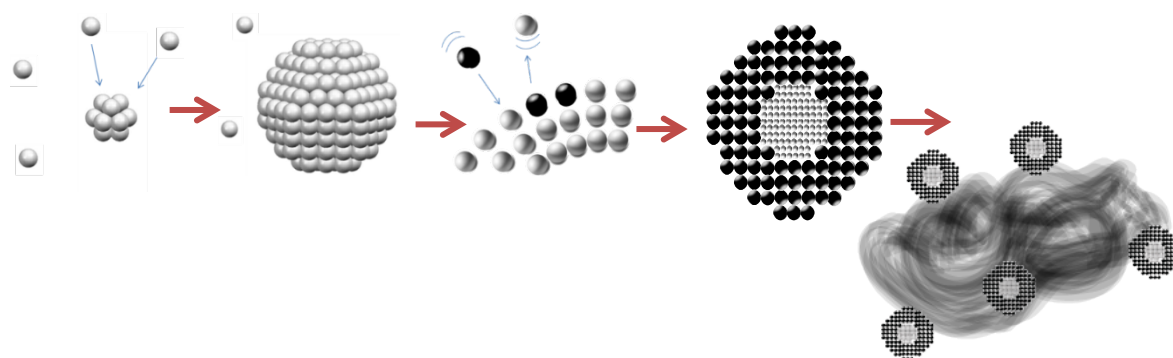


Figure S1 Illustration of particle synthesis involving galvanic replacement and particle adsorption on carbon support.

1.2 Predicting XRD reflections. The technique of choice to retrieve information on lattice properties is X-Ray Diffraction (XRD) ⁹. XRD, in comparison to other techniques such as electron beam microscopy, holds the advantage of analysing large samples thus providing an average over a large number of particles. Commonly XRD is used to identify the crystal structure(s) in a sample and the crystallite size. However peak analysis is rarely performed to its full potential. In core-shell nanoparticle analysis in particular, XRD can provide valuable insight into the macroscopic structure of a nanoparticle and the lattice strain arising from its particular synthesis. Commonly peak shift and broadening larger than what can be ascribed to effects of crystallite size, are being overlooked in literature or referred to as an effect of mixing of metals ⁹⁻¹².

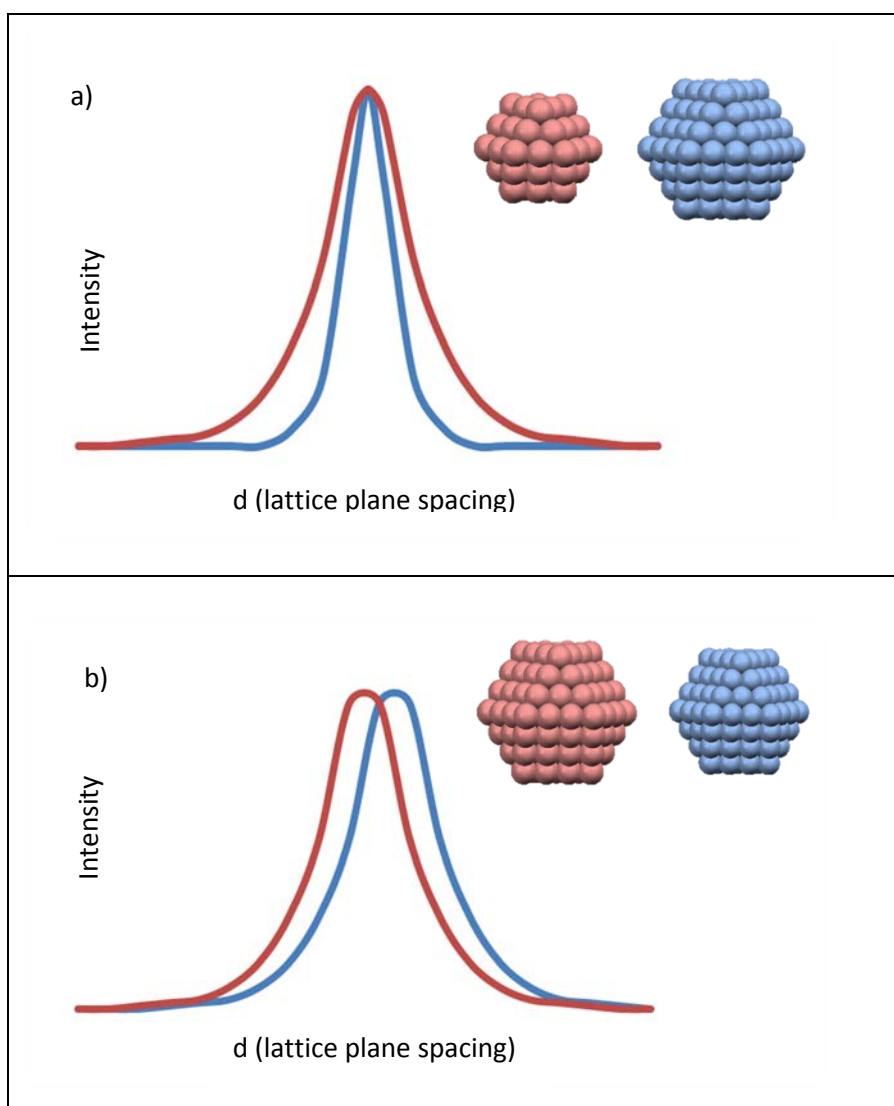
The intensity of a given reflection is largely determined by the form factor, i.e. the scatter from individual atoms, and the structure factor, i.e. the resultant wave from atoms in the unit cell. A core-shell particle consisting of two metals will result in scattering from the shell metal, the core metal and the interference between the two. The reflections from the shell will appear as those of a hollow sphere. In case the two constituting metals have a relatively large difference in atomic number Z , such as for Pt and Fe, the metal with the larger atomic number dominates the reflections to such an extent that the contribution from the metal with the smaller atomic number is not easily distinguished because its scattering intensity is a factor Z^2 smaller.

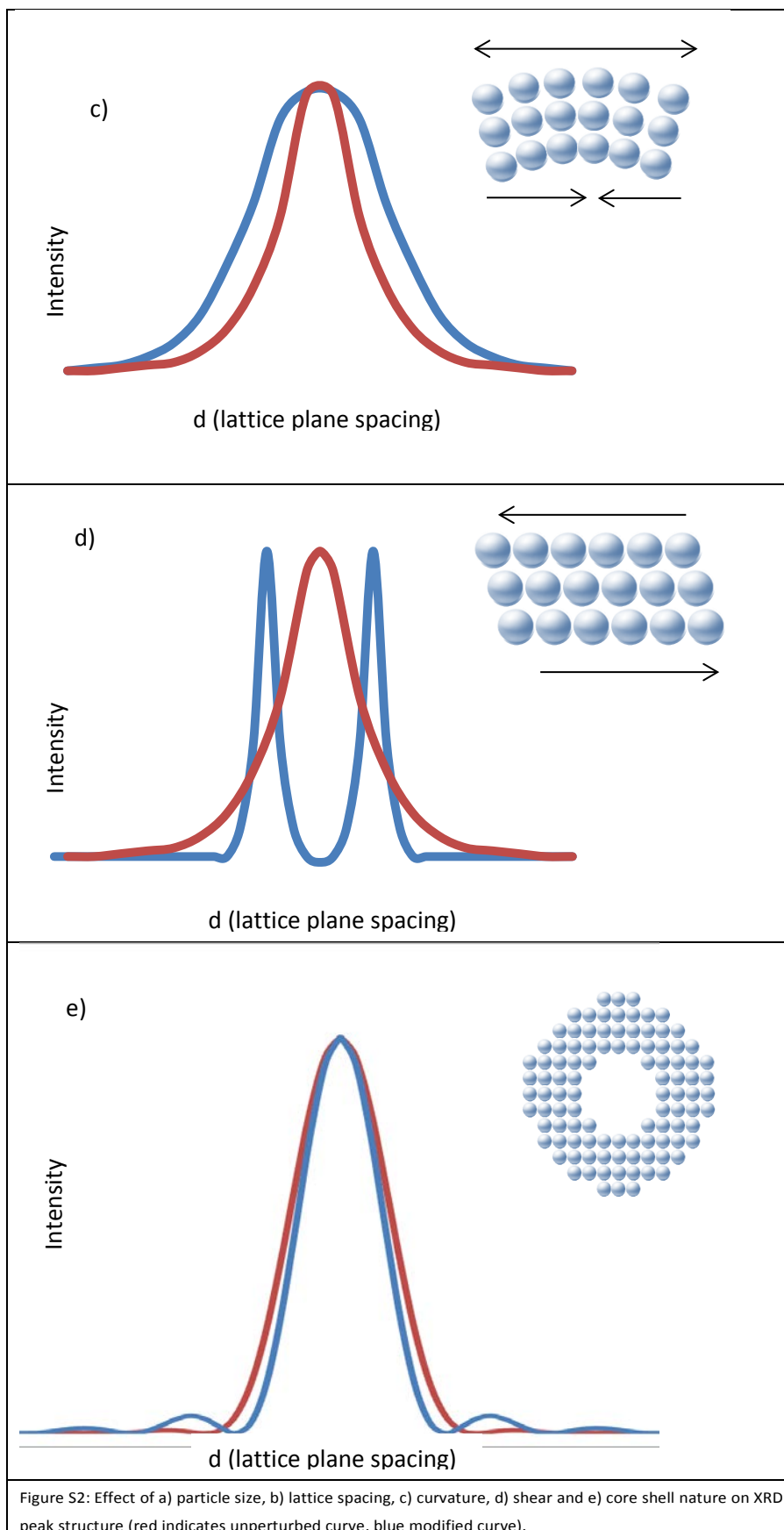
Particle size influences the peak width – a relation described by the Scherrer equation ¹³, illustrated in Fig. S2a. Furthermore, the smaller the particle the higher its Laplace pressure ¹⁴ which will lead to a compression of the particle and hence a peak shift to larger wave numbers, illustrated in Fig. S2b. Nanosized particles will therefore have a different peak position relative to bulk material ¹⁵. It can be assumed that a homogeneous internal pressure would act on a cubic lattice, however it is feasible that the pressure contributes to different amounts of strain in the various lattice planes resulting in different amounts of shift for different peaks. Keeping in mind that particle

size is determined both by the actual number of atoms making up the particle and the amount of lattice compression, both the peak position and the peak width might be affected.

Let us illustrate elongation strain by imagining a strip of a tensile metal. Pulling this strip of metal would cause elongation in the direction of the force and compression of the lattice in the vertical direction, shifting some peaks upwards and others downwards. Lattice compression would yield a peak shift towards higher angles meanwhile lattice elongation gives shift in the opposite direction (Figure S2b). If the strip would be bent the lattice would see an elongation and a compression simultaneously giving rise to a uniform peak broadening (Fig. 2c). A shear force, shifting successive lattice planes with respect to one another, causes the cubic lattice to deform into an orthorhombic lattice and causes peak shift or splitting (Fig. S2d).

The Fourier transform of a certain geometrical structure, e.g. sphere or cube, describes the shape of the reflection. A hollow sphere or a shell around a, for XRD invisible, core would be described by the Fourier transform of a sphere (with diameter D_1) from which the centre (a sphere with diameter D_2) has been subtracted¹⁶. The shape of a hollow sphere (with shell thickness of $\frac{D_1-D_2}{2}$) remains. The structure factor of such hollow sphere would result in a distribution with abnormally long tails compared to a solid sphere with the same diameter, taking into account that the oscillations in the tail even out if for a distribution of shell thicknesses⁹. This is illustrated in Fig. S2e, the cartoon being merely a rough sketch of reality.





The lattice constants of Pt, Fe, Ni and Cu are 3.920, 2.866, 3.524 and 3.615 Å respectively, hence, fitting Pt onto the core metal will cause lattice contraction. One monolayer of Pt on top of bulk Fe, Ni or Cu would theoretically generate a compressive strain of

$$\varepsilon_{ML} = \frac{d_{Pt} - d_{Me}}{d_{Pt}} \quad (\text{Eq. S1})$$

where d is the lattice constant. The peak displacement generated in the XRD diffractograms are relative to the Platinum lattice, hence it is useful that the formula similarly describes the strain of the Platinum lattice if it were to follow the core metal lattice. Throughout this paper strain means lattice contraction (reduction of interatomic distance) and to avoid confusion the numbers for strain are presented as negative numbers since it represent a reduction in lattice spacing.

2. Method

2.1. Chemicals. Surfactant AOT ($C_{20}H_{37}NaO_7S$, 98%) or sodium bis(2-ethylhexyl) sulphosuccinate, heptane (C_7H_{14} , $\geq 99.9\%$), chloroplatinic acid hydrate ($H_2PtCl_6 \cdot 6H_2O$, $\geq 99.9\%$), iron chloride hexahydrate ($FeCl_3 \cdot 6H_2O$, $\geq 97\%$), copper chloride ($CuCl_2$, $\geq 99.9\%$), nickel chloride ($NiCl_2$, $\geq 98\%$), sodium borohydride ($NaBH_4$, $\geq 99\%$), tetrahydrofuran (THF $\geq 99.9\%$), hydrochloric acid (HCl, 37%) and acetone (CH_3COCH_3 , $\geq 99.9\%$) all used as received from Sigma Aldrich. Nafion solution (5 wt % ; 250 ml) and carbon support (Vulcan XC-72R) were purchased from Quintech. For all sample preparations, reagent-grade water produced by a Milli-Q ultrapure purification system from Millipore BV was used.

2.2. Synthesis of core-shell particles. The synthesis of transition metal cores was achieved by reduction of a transition metal salt by sodium borohydride in the aqueous phase of a bi-continuous micro-emulsion. A bi-continuous micro-emulsion was prepared by mixing 56 wt% Na-AOT, 20 wt% milli-Q water and 24 wt% heptane¹⁷. One micro-emulsion, in which the transition metal precursor was dissolved in the water phase, was mixed with a second micro-emulsion containing reducing agent, resulting in the formation of transition metal cores, its size being controlled by the size of the water channels in the emulsion. Cores with three different types of metals were synthesized; Fe, Ni and Cu. After completion of the reduction process a third micro-emulsion containing Pt salt precursor is added slowly to the core emulsion. The subsequent galvanic replacement is left to proceed for at least 2 hours after which addition of 60 wt% carbon support (Vulcan XC72) and a washing procedure of 6 steps follows. Washing is intended to remove heptane and surfactant from the particles. In the acid washing step any uncoated core metal and core-shell particles that have not adsorbed to the carbon support are washed away.

In the first two washing steps THF is added dropwise to the dispersion during stirring followed by ultra-sonication for 10 min to remove the surfactant from the particle surface and centrifugation at 6000 rpm for 10 min. In step 3-4 the particles are washed with 50 ml 1 M HCl in order to dissolve any uncoated core particles. More than two acid washing steps has proven not to remove any more (core)material from the sample. In the last two steps the particles are washed with 50 ml Milli-Q water. The powder is left to dry at 60 °C for 12 h.

This method of producing bimetallic core-shell type particles and a systematic way of determining such structure was published in our earlier work¹⁸ and is illustrated in Fig. S1. Core-shell synthesis through galvanic replacement has also been previously described but this work adds the use of galvanic replacement in a microemulsion synthesis^{10,19}.

2.3. Synthesis of pure Pt reference particles. Samples with pure Pt particles on carbon were made similarly to the core-shell particles but using Platinum as core metal and skipping the step of galvanic replacement. Analogous to the core-shell particles the pure Pt particles were supported on carbon and washed in six steps including acid washing.

2.4. Instrumentation and Measurements. The particle sizes were all determined using Dynamic Light Scattering (DLS) using a ZetaSizer Nano ZS from Malvern Instruments and Transmission Electron Microscopy (TEM) using a JEOL JSM 2012. With DLS the particle size is measured before the addition of carbon support whereas the particles are adsorbed on the carbon support when measured with TEM. The final composition of the particles was evaluated using Inductively Coupled Plasma Atomic Emission Spectroscopy (ICP-AES) by dissolving approximately 25 mg of the particles in Aqua Regia, diluting it with Milli-Q water to 50ml and analysing it using a PerkinElmer Optima 5300DV. Particle composition was also analysed with Energy Dispersive Spectroscopy (EDS) using a JEOL JSM-6010LA InTouchScope. All samples were characterized by X-Ray Diffraction (XRD) with Co $K\alpha$ radiation of wavelength 1.79 Å using a Bruker AXS D8 Discover.

To make sure that any peak displacement in XRD is not an artefact of axis offset – sample height in XRD – measurements with a calibration standard at lower and higher axis offset was made resulting in a maximum peak shift of $\pm 0.5\%$.

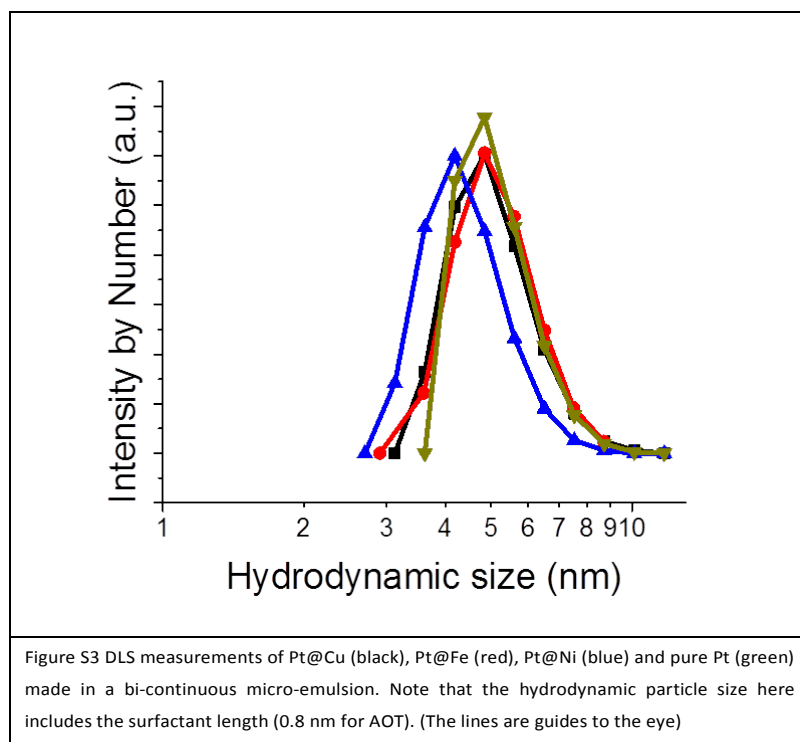
2.5. Electrochemical measurements. Cyclic voltammetry (CV) and hydrodynamic voltammetry (HV) were performed in a standard single 3-electrode cell using a Reversible Hydrogen Electrode as reference electrode and a Pt mesh as counter electrode. A Rotating Disk Electrode (RDE) with a 5 mm in diameter glassy carbon disk and hence an electrode area of 0.198 cm² from PINE Research Instrumentation was used for the hydrodynamic measurements. To make the catalyst ink layers on the electrode 13 µl of catalyst ink was drop casted on the disk, containing 6.5 µg of catalyst material (i.e. carbon + core-shell particles) out of which 40-70 wt% was carbon. All experiments were conducted in a 0.1 M HClO₄ solution saturated with Ar for the cyclic voltammetry and O₂ for the hydrodynamic voltammetry using rotation speeds of 400, 900, 1600 and 2500 rpm²⁰. Scan speed for CV was 50 mV and 5mV for HV.

Since the surface area of Platinum, A , covered by one hydrogen atom is proportional to the lattice constant squared, d^2 , for a cubic lattice, the relative change in area with lattice strain can be calculated according to Eq. 2, assuming that each lattice site is maximally occupied with one hydrogen.

$$\frac{\Delta A}{A} = \frac{d^2 - d_0^2}{d_0^2} \quad \text{Eq. S2}$$

Where d_0 represents the unstrained lattice constant. If the lattice is strained, the lattice constant will be changed and hence the surface area per atom will change (see Table S1), bearing in mind that the assumption of one hydrogen per atom may at some point be lost for strained lattices.

3. Results and Discussion



The mechanism of particle growth in bi-continuous micro-emulsions has been reported previously by our group¹⁷. The mechanism of galvanic replacement has been described in literature previously^{10, 19, 21}.

Upon mixing of the micro-emulsions containing reducing agent and core precursor, most of the metal core nanoparticles are formed within minutes, and the reaction is complete after 2 h. Leaving the reaction to proceed longer than 2 h does not result in considerably higher yield of core particles. The ratio Pt:Me, where Me stands for the core metal used, in the final catalyst could be varied by the concentrations of the precursors. Also for the minimum time required for the shell to form in the galvanisation step was approximately 2 h. Leaving the core particles in the Platinum ion rich solution did not yield pure Pt particles even for an extended amount of time. Considering the time scales for (1) primary particle formation, (2) shell formation through galvanic replacement

and (3) adsorption of particles onto carbon support, the latter is the slowest process. The adsorption time needed was approximately 8 hours. Thus, Initiating the washing procedure too soon after the carbon support is added results in very low contents since formed particles simply are washed away. The adsorption of Pt on the carbon is indeed expected to be the time limiting step since the surfactant present competes in adsorbing and may slow down the adsorption of Pt onto carbon. Nevertheless, experiments also show that the surfactants can function as anchors between the particles and the carbon support hindering agglomeration. For ratios smaller than Pt:Me 1:2 (at) for a particle size of 3 nm the Pt content is too low in order to form a continuous shell. Hence the smallest fraction of Platinum used here is Pt:Me 1:1.

Table S1 Predicted maximum strain ($\Delta d/d$) considering one monolayer of Pt on top of Fe, Cu and Ni (Eq. S1) and predicted decrease in ECSA ($\Delta A/A$) with lattice spacing (Eq. S2).

	$\Delta d/d$	$\Delta A/A$
Pt@Fe	- 26.8 %	- 60.7 %
Pt@Cu	- 7.8 %	- 16.2 %
Pt@Ni	- 10.1 %	- 21.2 %

Table S2 Results table for one of each sets of particle types

Sample	Atomic ratio Pt:Me	Composition wt% (C:Pt:Me)	Particle size, d
Pt@Ni	2:1	72:25:3	2.7 ± 0.6 nm
Pt@Fe	5:1	58:41:1	3.2 ± 0.6 nm
Pt@Cu	2:1	54:41:5	3.2 ± 0.6 nm
Pt	-	60:40	3.2 ± 0.6 nm

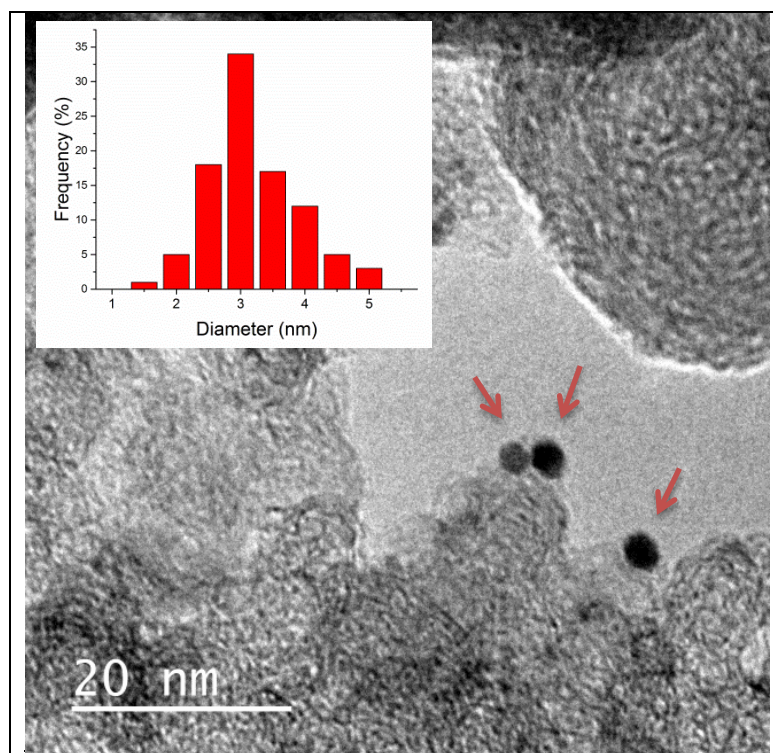
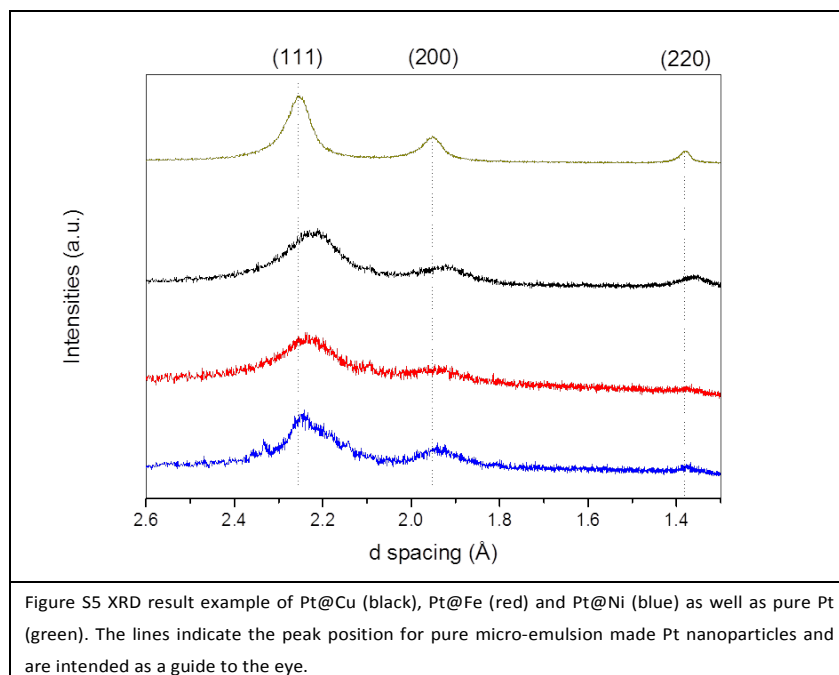
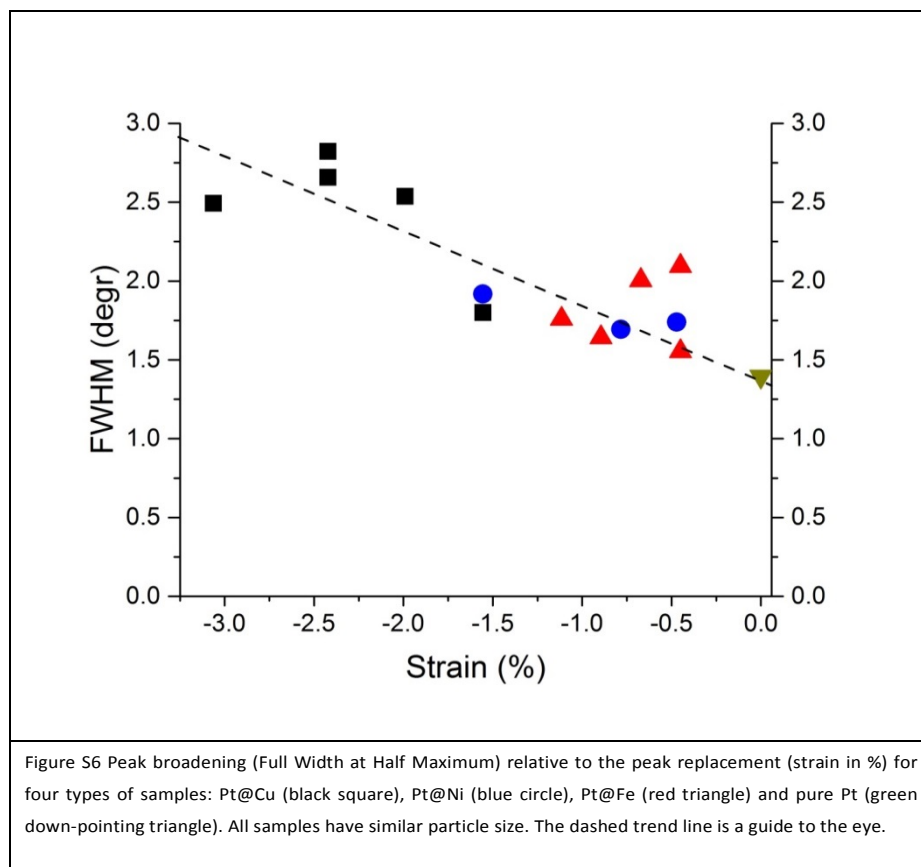


Figure S4 TEM picture of Pt@Cu particles supported by high surface area carbon (Vulcan XC72). The red arrows indicate the locations of the spherical particles and the surrounding grey structure is the carbon. Inset figure is a histogram showing particle size distribution from TEM.

All core-shell samples show a lattice shift representing lattice contraction compared to our pure Pt particles. The small peaks at $d=2.1$ Å for Pt@Cu and Pt@Fe could not unambiguously be identified, likewise for the peak at $d=2.3$ Å for Pt@Ni. They could possibly originate from interference between the two metals. Another possibility is impurities. The Pt@Ni sample shown in Fig S5 is the Pt@Ni sample with the highest activity and thinnest shell. For the samples with thicker shell no peaks at $d=2.3$ Å were found. Due to the synthesis method and the voltammetric results any surface Ni atoms are not a likely cause of these additional peaks. It is not trivial to rule out that possible impurities or subsurface alloying between Pt and Ni in this particular sample have an influence on the catalytic activity but generally such influence is expected to be of marginal importance. The largest peak displacement (3%) was seen for the Pt@Cu (2:1) samples.

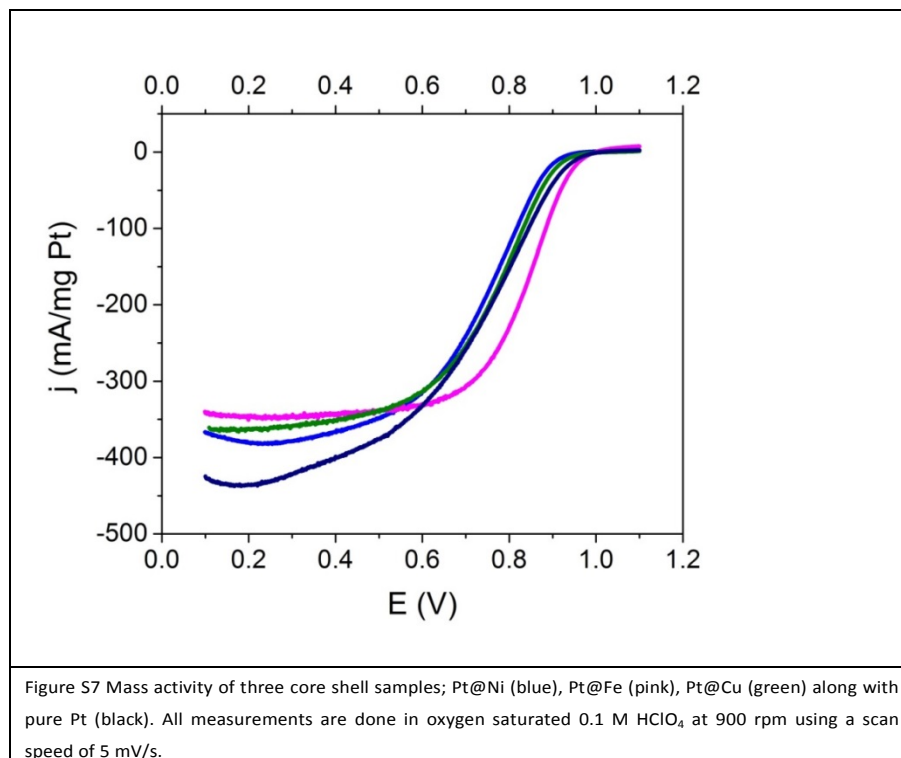


In Fig. S6 it is shown that the samples with the most compressed Platinum lattice also show the largest peak broadening, i.e. a larger Full Width at Half Maximum (FWHM) value. Note that all particles, including pure Pt, have a very similar particle size (Table S2).



From the multiple-cycle voltammograms performed in deaerated electrolyte, information can be extracted about the surface dominating species and whether it is completely covering the core. In the event that some particles with an uncovered core would have persisted after the acid washing, they would leach out upon atom rearrangements driven by the potential cycling. For at least 100 cycles no significant persisting change in the voltammograms was observed for any of the presented samples, i.e. for shell to core atomic ratios above 1:2. Moreover, changes seen in the first few cycles, usually ascribed as being surface cleaning or even surfactant removal, are not different from pure Pt samples²².

For the hydrodynamic voltammograms (Fig. S7) measured in oxygen saturated electrolyte the catalytic activity towards the oxygen reduction reaction is studied. Although the exact mechanism of the oxygen reduction reaction is not yet fully explained, oxygen can be reduced via a 2-electron reduction pathway to H_2O_2 or via a 4-electron reduction pathway to H_2O , the latter being the preferred route in fuel cell applications³. Since Pt-based oxygen reduction electrocatalysts tend to predominantly favour the desired 4-electron reduction pathway, the selectivity in terms of reduction pathway of the catalysts has not been further studied here²³.



Regarding the washing procedure the acidic washing step is needed to ensure core-shell structure as mentioned above, however it efficiently washes away surfactant molecules acting partly as anchors between the particles and the carbon support. Too much remaining surfactant lowers the conductivity of the sample and might limit the accessibility of the catalytic particle surface. However, extensive removal appears to induce loosely bound particles and hence lead to agglomeration of particles. This requires further optimization of the procedure.

We have managed to generate core-shell particles with lattice strains ranging from 0.5% up to 3% and showed how the strain affects the ability to catalyse the ORR. For Pt@Fe and Pt@Cu we observe a decrease in activity with lattice strain and the contrary for Pt@Ni, illustrated in Fig. S8.

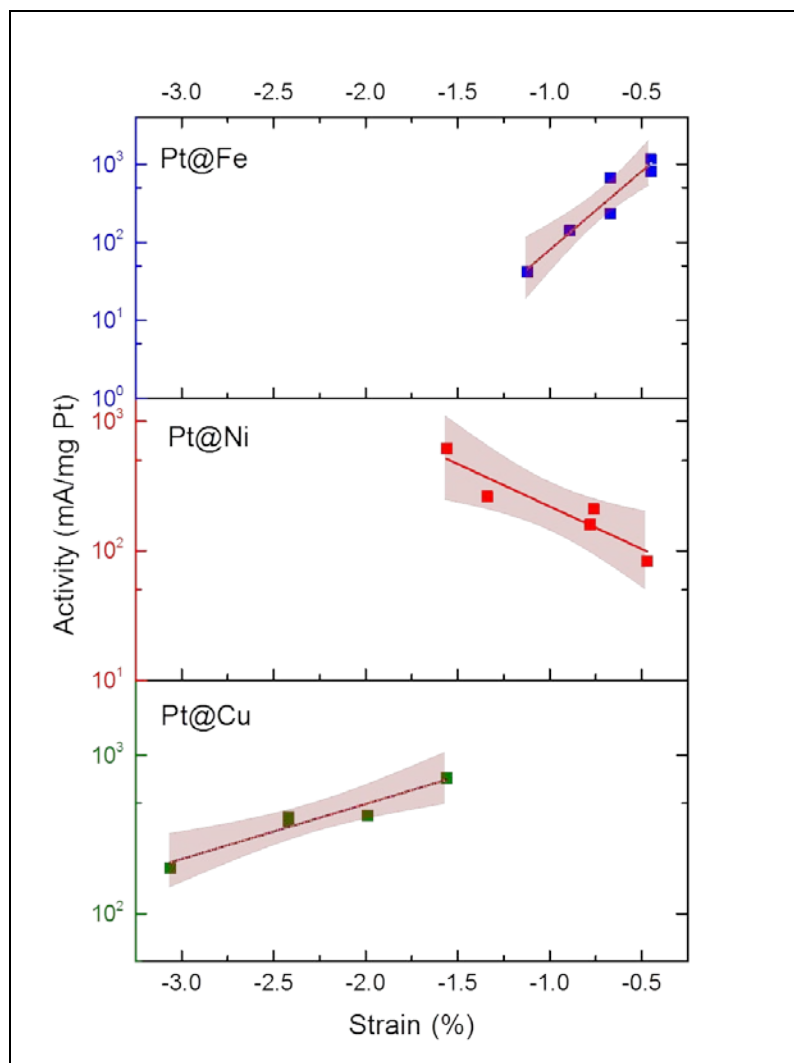


Figure S8 The exponential correlation between strain and oxygen reduction activity for the three different types of core-shell samples. Each observation is one unique particle sample for which activity has been measured using RDE and strain by using XRD. The fitted lines are a guide to the eye and the shaded area is the 95% confidence band.

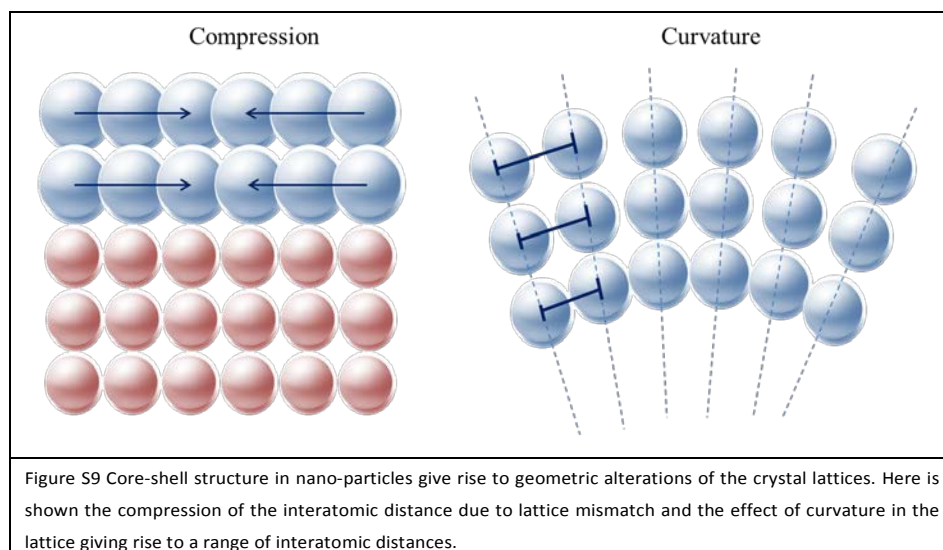


Figure S9 Core-shell structure in nano-particles give rise to geometric alterations of the crystal lattices. Here is shown the compression of the interatomic distance due to lattice mismatch and the effect of curvature in the lattice giving rise to a range of interatomic distances.

Notes and References

1. J. Zhang, *PEM Fuel Cell Electrocatalysts and Catalyst Layers*, Springer, London, UK, 2008.
2. J. K. Nørskov, J. Rossmeisl, A. Logadottir, L. Lindqvist, J. R. Kitchin, T. Bligaard and H. Jonsson, *J. Phys. Chem. B*, 2004, **108**, 17886-17892.
3. M. T. M. Koper, *Chemical Science*, 2013, **4**, 2710-2723.
4. B. H. J. K. Nørskov, *Advances in Catalysis*, 2000, **45**, 71-129.
5. E. Santos, P. Quaino and W. Schmickler, *Electrochimica Acta*, 2010, **55**, 4346-4352.
6. Y. Cai and R. R. Adzic, *Advances in Physical Chemistry*, 2011, **2011**, 1-16.
7. D. A. J. R. T. Biegler, R. Woods, *Journal of Electroanalytical Chemistry*, 1971, **29**.
8. P. Trasatti, *Pure & Appl. Chem.*, 1991, **63**, 711-734.
9. R. Popescu, P. Leidinger, C. Kind, C. Feldmann and D. Gerthsen, *Journal of Nanoparticle Research*, 2013, **15**.
10. A. Sarkar and A. Manthiram, *Journal of Physical Chemistry C*, 2010, **114**, 4725-4732.
11. C. Li and Y. Yamauchi, *Physical chemistry chemical physics : PCCP*, 2013, **15**, 3490-3496.
12. J. M. Sieben, V. Comignani, A. E. Alvarez and M. M. E. Duarte, *International Journal of Hydrogen Energy*, 2014, **39**, 8667-8674.
13. E. Zolotoyabko, *Basic Concepts of X-Ray Diffraction*, Wiley, Weinheim, Germany, 2014.
14. G. J. M. Koper, *An introduction to Interfacial Engineering*, VSSD, Delft, The Netherlands, 2009.
15. B. D. Cullity, *Elements of X-Ray Diffraction*, Addison-Wesley Publishing Company Inc., Massachusetts, 1956.
16. H. L. H. Ibach, *Solid-State Physics: An Introduction to Principles of Materials Science*, Springer-Verlag Berlin Heidelberg, 2003.
17. E. Negro, R. Latsuzbaia and G. J. Koper, *Langmuir : the ACS journal of surfaces and colloids*, 2014, **30**, 8300-8307.
18. E. Westsson and G. Koper, *Catalysts*, 2014, **4**, 375-396.
19. B. Geboes, I. Mintsouli, B. Wouters, J. Georgieva, A. Kakaroglou, S. Sotiropoulos, E. Valova, S. Armanyan, A. Hubin and T. Breugelmans, *Applied Catalysis B: Environmental*, 2013.
20. Y. Garsany, J. Ge, J. St-Pierre, R. Rocheleau and K. E. Swider-Lyons, *Journal of the Electrochemical Society*, 2014, **161**, F628-F640.
21. A. Papaderakis, I. Mintsouli, J. Georgieva and S. Sotiropoulos, *Catalysts*, 2017, **7**, 80.
22. S. E. Kleijn, S. C. Lai, M. T. Koper and P. R. Unwin, *Angew Chem Int Ed Engl*, 2014, **53**, 3558-3586.
23. A. Kulkarni, S. Siahrostami, A. Patel and J. K. Nørskov, *Chemical reviews*, 2018, **118**, 2302-2312.